Photochemical & Photobiological Sciences

PAPER



Cite this: *Photochem. Photobiol. Sci.*, 2019, **18**, 2142

# Optimized synthesis of luminescent silica nanoparticles by a direct micelle-assisted method†

Benedetta Del Secco, [a] Luca Ravotto, [b] Tatiana V. Esipova, [b] Sergei A. Vinogradov, *[b] Damiano Genovese, [a] Nelsi Zaccheroni, [a] Enrico Rampazzo *[a] and Luca Prodi *[a]

Received 24th January 2019,
Accepted 1st April 2019

DOI: 10.1039/c9pp00047j

rsc.li/pps

Silica nanoparticles (NPs) are versatile nanomaterials, which are safe with respect to biomedical applications, and therefore are highly investigated. The advantages of NPs include their ease of preparation, inexpensive starting materials and the possibility of functionalization or loading with various doping agents. However, the solubility of the doping agent(s) imposes constraints on the choice of the reaction system and hence limits the range of molecules that can be included in the interior of NPs. To overcome this problem, herein, we improved the current state of the art synthetic strategy based on Pluronic F127 by enabling the synthesis in the presence of large amounts of organic solvents. The new method enables the preparation of nanoparticles doped with large amounts of water-insoluble doping agents. To illustrate the applicability of the technology, we successfully incorporated a range of phosphorescent metalloporphyrins into the interior of NPs. The resulting phosphorescent nanoparticles may exhibit potential for biological oxygen sensing.

## Introduction

Silica nanoparticles (NPs) exhibit potential for applications in many fields,[1–3] including imaging,[4,5] drug delivery,[6,7] sensing[8] and catalysis.[9] Most of their versatility originates in the characteristics of silica itself; this material is hydrophilic and non-toxic,[10,11] and its chemistry is well established. Silica nanomaterials can be produced using several strategies, which make it possible to build particles of a desired size, shape and even mesoporosity[12] and bio-erodibility.[13,14]

The synthetic approaches, based on the liquid phase, can be classified into three main families: (i) the Stöber method,[15–17] (ii) the reverse micelles approach (water-in-oil methods),[18–20] and (iii) those preparative pathways assisted by templates such as direct micelles.[21–23] Functions can be conferred to NPs according to their mesoporosity, dimension and shape and by the presence of a doping agent. The possible doping species can be a catalyst, receptor, chemosensor, drug or dye, depending upon the demands of the application. However, the choice of the doping agent(s) is practically limited by its solubility in the reaction milieu. Therefore, solubility is a key property, which determines the possible doping level and the quality of incorporation. Each approach presents its own limitations. For example, the Stöber synthesis requires the solubilisation of the doping moieties in an alcohol–water mixture, and it is therefore suitable only for the incorporation of polar species. Solubility restrictions in the reverse microemulsion approach (water-in-oil) are even more severe, since only molecules with reasonable solubility in water can be efficiently incorporated into the core of reverse micelles and, consequently, in NPs.

The strategy based on the aqueous solutions of surfactants, exploiting the template capability of direct micelles, can employ surfactants of low or high molecular weight, but these also present similar solubility restrictions: the components for doping or surface functionalization must be sufficiently soluble in the aqueous media when the concentrations of the surfactants are relatively low.

The role of solubility in the design of silica nanomaterials has been the focus of our research in the recent few years. We have already demonstrated, for example, that following the Stöber preparation, less polar dyes spontaneously accumulate in the center of a nanoparticle, especially at high doping concentrations, which leads to intermolecular interactions, resulting in emission self-quenching, energy or electron transfer processes.[24]

More recently, we focused on silica core/PEG shell nanoparticles, which can be obtained through one-pot direct micelle-assisted template synthesis, leading to a range of luminescent materials[25,26] for applications in the *in vitro*[27] and

[a]*Department of Chemistry "Giacomo Ciamician", University of Bologna, Via Selmi 2, 40126 Bologna, Italy. E-mail: enrico.rampazzo@unibo.it, luca.prodi@unibo.it*
[b]*Departments of Biochemistry and Biophysics and of Chemistry, University of Pennsylvania, Philadelphia, PA 19104, USA. E-mail: vinograd.upenn@gmail.com*

†Electronic supplementary information (ESI) available: Details of experimental procedures, Dynamic Light Scattering of micelle and nanoparticles suspension, TEM images and photophysical characterization. See DOI: 10.1039/c9pp00047j

*in vivo*[28,29] optical and photoacoustic[30] imaging, as chemosensors[31] or as electrochemiluminescent probes.[32]

The incorporated dyes are often large hydrophobic molecules or metal complexes possessing expanded aromatic structures, which promote intermolecular π-stacking and limit solubility in aqueous environments.

To overcome this limitation, herein, we report a new improved Pluronic F127-based synthetic strategy, which in its original form is known to be able to tolerate only small amounts of organic solvents (*e.g.* DMSO or DMF) (Fig. 1). The new method, in contrast, enables syntheses in environments containing large quantities of organic solvents, which is highly beneficial for the incorporation of hydrophobic dopants into the interior of the nanoparticles. In this work, we chose to use phosphorescent metalloporphyrins as model dopants with varying degrees of π-extension. First, porphyrins are known to be difficult-to-solubilize targets, often exhibiting great propensity toward π-stacking and aggregation. On the other hand, porphyrins and their metal complexes form a group of versatile dyes with exceptionally rich optical and electrochemical properties, which present interest for applications in many areas of technology and medicine, from catalysis to biomedical imaging and phototherapy (Fig. 1). Phosphorescent Pt and Pd porphyrins, in particular, have been broadly used as luminescent dyes for the construction of molecular probes for optical sensing of oxygen in biological systems.[33,34] In order to ensure aqueous solubility, tune the sensitivity of the phosphorescence into the optimal range for biological oxygen detection and simultaneously make porphyrin signals selective for oxygen in complex biological environments, porphyrins or any other phosphorescent dyes need to be incorporated into a protective shell with inert hydrophilic periphery. At the present time, probes with the required properties that allow truly quantitative oxygen measurements *in vivo* comprise a set of Pt or Pd porphyrin-dendrimers with PEGylated periphery (PEG = polyethyleneglycol).[35–38] However, the synthesis of porphyrin dendrimers is not simple and may present an obstacle for the dissemination of the technology. On the other hand, simpler probes, based on phosphorescent molecules equipped with various solubilizing groups and/or incorporated into nanoparticles do not have the ability to sense oxygen quantitatively, which is due to non-specific interactions of the probes with various biological macromolecules.[39,40] Thus, phosphorescent metalloporphyrins incorporated inside silica nanoparticles with PEGylated exterior may be viewed as a simpler, less expensive alternative to dendritic oxygen probes. The synthetic methodology described herein constitutes the first step towards such oxygen probes as well as other sensors for biological analytes.

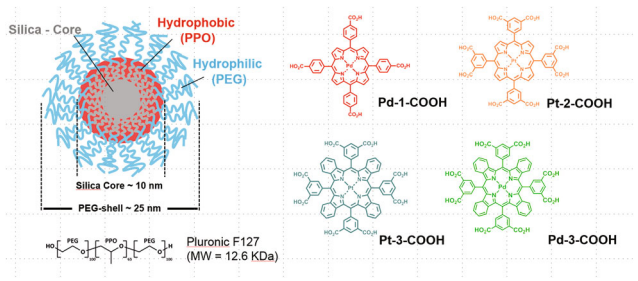


**Fig. 1** Scheme of the structure of core–shell silica–nanoparticles obtained using the Pluronic F127-based synthetic strategy. Molecular structures of Pluronic F127 surfactant and of the porphyrin dyes used as doping agents in this work (PPO: polypropylene oxide; PEG: polyethylene glycol).

# Experimental

## Materials and methods

All reagents and solvents were used as received without further purification. Non-ionic surfactant Pluronic® F127, tetraethyl orthosilicate (TEOS, 99.99%), tetramethyl orthosilicate (TMOS, >99%), chlorotrimethylsilane (TMSCI, 98%), hydrochloric acid (fuming, >37%), (3-aminopropyl)triethoxysilane (98%), 2-chloro-4,6-dimethoxy-1,3,5-triazine (CDMT, 97%), 4-methylmorpholine (NMM, 99%), reagent grade dimethylformamide (DMF), tetrahydrofuran (THF) and acetic acid (99.7%) were purchased from Sigma-Aldrich. NaCl was purchased from Fluka. Metallo-porphyrin **Pd-1-COOH** (Pd(II) *meso*-tetra (4-carboxyphenyl)porphyrine) was purchased from Frontier Scientific, Inc. Metallo-porphyrin **Pt-2-COOH**, **Pt-3-COOH** and **Pd-3-COOH** (Fig. 1) were synthesized as previously reported.[35] A Millipore Milli-Q system was used for the purification of water (resistivity 18 MΩ).

**Dialysis experiments.** Filtration of particle solutions was done when necessary using a Millipore Durapore or RC filters (0.22, 0.45 pm). Dialysis was performed against water at room temperature under gentle stirring with regenerated cellulose dialysis tubing (Sigma, mol wt. cut-off >12 000 Da, avg. diameter 33 mm).

**Dynamic light scattering measurements (DLS).** The determination of the hydrodynamic diameter distribution of the NPs was carried out through Dynamic Light Scattering measurements employing a Malvern Nano ZS instrument equipped with a 633 nm laser diode. Samples were housed in disposable polystyrene cuvettes of 1 cm optical path length, using water as the solvent. Pdl (Polydispersion Index) indicates the width of the DLS hydrodynamic diameter distribution. In case of a mono-modal distribution (Gaussian) calculated by means of cumulant analysis, Pdl = $(\sigma/Z_{avg})^2$, where $\sigma$ is the width of the distribution and $Z_{avg}$ is the average diameter of the particle population.

**Photophysical measurements.** All NP dispersions showed very weak light scattering and were treated from the photophysical point of view as any solution of molecular species. DLS measurements showed no aggregation of the NPs, even after several months. UV-vis absorption spectra were recorded at 25 °C by means of a PerkinElmer Lambda 45 spectrophotometer. Emission spectra and lifetime decay were recorded using a HORIBA Jobin Yvon Fluoromax-4 spectrofluorimeter. Photophysical characterization in the absence of oxygen was

carried out on samples of dye solutions and NP dispersions after degassing them by freeze–pump–thaw cycling ($P = 10^{-9}$ Bar; liquid nitrogen as cooling medium) in a custom made quartz cuvette.

**Transmission electron microscopy measurements.** A Philips CM 100 TEM operating at 80 kV was used. For TEM investigations, a holey carbon foil supported on conventional copper microgrids was dried under vacuum after deposition of a drop of NP solution diluted with water (1 : 50). We obtained the size distribution by analysing images with a block of several hundreds of NPs.

### Synthetic procedures

**General procedure for the functionalization of porphyrins with triethoxysilane.** The amounts of reagents and solvent used for the functionalization of porphyrins with triethoxysilane moieties are summarized in Table 1. Two synthetic protocols were used depending on the porphyrin structure.

**Protocol 1**: **Pd-1-COOH** (40 mg, 1 eq.) was dissolved in a 20 mL scintillation glass vial with 4 mL of DMF. CDMT (31.6 mg, 4.1 eq.), NMM (37.6 μL, 8.1 eq.) and APTES (42.1 μL, 4.1 eq.) were added to this solution. Upon the addition of NMM and APTES, a red slurry formed and quickly dissolved. The reaction mixture was stirred overnight in the dark. The mixture reaction containing the conjugate **Pd-1-APTES** was directly used for the nanoparticle synthesis without further purification.

**Protocol 2** (metallo-porphyrins **Pt-2-COOH**, **Pt-3-COOH** and **Pd-3-COOH**): In a round bottom flask, the carboxylic porphyrins and CDMT were dissolved in DMF. NMM was then added and the reaction mixture was stirred at 0 °C for 2 hours. A second aliquot of NMM was then added, followed by APTES, and the reaction was stirred at room temperature overnight in dark conditions. Finally, the reaction mixture containing the triethoxysilane-functionalized dyes (metallo-porphyrins **Pt-2-APTES**, **Pt-3-APTES** and **Pd-3-APTES** respectively) was directly used for the NP synthesis.

**Nanoparticle synthesis.** A precise amount of porphyrin dye mixture (obtained by protocol 1 or protocol 2) was added to a mixture of 100 mg of Pluronic F127, NaCl (68.6 mg), organic solvent and 1 M acetic acid. The total volume of the organic solvent and 1 M acetic acid was 1.55 mL. Various volumes of porphyrin dye mixtures were added to obtain the desired NPs doping level (0.5%, indicated as %mol of dye *vs.* mol TEOS). The mixture was then solubilized under magnetic stirring at 25 °C, and TEOS (180 μL, 0.80 mmol) was added to the resulting homogeneous solution followed by TMSCI (10 μL, 0.08 mmol) after 180 min. The mixture was kept under stirring in the dark for 24 h at 25 °C before dialysis. The dialysis purification was carried out against water and finally diluted to a total volume of 10 mL with water.

Table 1 Amounts of reagents and solvents used for the triethoxy functionalization of the porphyrin dyes used in this study

| Porphyrin, mg (mmol) | APTES, μL (mmol) | CDMT, mg (mmol) | NMM, μL (mmol) | DMF, mL |
|---|---|---|---|---|
| **Pd-1-COOH**, 40 (0.045) | 43 (0.184) | 32 (0.184) | 41 (0.368) | 4 |
| **Pt-2-COOH**, 17 (0.013) | 21 (0.09) | 16 (0.09) | 20 (0.18) | 1.3 |
| **Pt-3-COOH**, 13 (0.011) | 25 (0.11) | 19 (0.011) | 24 (0.216) | 1.5 |
| **Pd-3-COOH**, 12 (0.008) | 17 (0.071) | 12 (0.071) | 16 (0.142) | 1 |

## Results and discussion

Among all known synthetic strategies for the preparation of silica nanoparticles, we are interested in the method based on the use of aqueous solutions of surfactants, *i.e.*, exploiting the template capability of direct micelles. Within this method, two main approaches can be distinguished, namely, employing a low or a high molecular weight surfactant. In the first case, a low molecular weight surfactant (AOT: dioctylsulfosuccinate, Tween) was solubilized in water at a higher concentration with respect to its c.m.c. to form a dispersion of micelles ($d_H$ = 10 nm). The formation of silica NPs in these experimental conditions is generally achieved using lipophilic alkoxysilanes (*e.g.* vinyltriethoxysilane) as precursors of an organo-silica matrix. These lipophilic molecules, in fact, can undergo repartition in the micelle cores, where condensation reactions occur leading to organo-silica formation. The resulting systems are often named ORMOSIL (ORganically MOdified SILica)[23] nanoparticles, and for their doping, dyes or surface functionalization components that have sufficient solubility in quite dilute aqueous solution of a surfactant must be used.

The synthetic strategies employing a high molecular weight surfactant are fewer and most of them exploit A–B–A triblock copolymers such as Pluronic (or Polaxomer). These surfactants have a general molecular formula of $PEO_x$–$PPO_y$–$PEO_x$ (PEO, polyethyleneglycol; PPO, polypropyleneoxide), with coefficients $x$ and $y$ determining their overall polarity and aggregation behaviour in water. In particular, the high molecular weight Pluronic F127 surfactant is the most used in the fabrication of silica NPs due to the capability of its aggregates (or co-aggregates) to act as templates in the formation of NPs (a structure also called cross-linked micelles). The versatility of this approach is huge, since it provides a one-pot strategy to obtain extremely monodisperse NPs with a core–shell silica–PEG structure (hard diameter = 10–12 nm; hydrodynamic diameter = 20–30 nm). In the preparation of luminescent materials, this strategy shows solubility restrictions on the doping dye(s) that are comparable to the ones tested in the ORMOSIL preparation, but the higher surfactant aggregate inner polarity makes the use of tetraalkoxysilane precursors possible, leading to a silica network with a higher reticulation level. This latter aspect is very important in the preparation of oxygen sensors, since the reticulation degree has an effect on the diffusion of the molecular oxygen inside the silica matrix.

### Solvent screening of the hydrodynamic behaviour of Pluronic F127 aggregates in water/organic solvent mixtures

Our first investigation of this synthetic method in the presence of a large amount of organic solvent was to evaluate the effect

 

of few organic solvents on the hydrodynamic behaviour of Pluronic F127 aggregates. We considered the Pluronic F127 concentration usually employed in the 1 M acetic acid synthetic protocol (5.1 mM), and the hydrodynamic behaviour of Pluronic F127 aggregates in solution in the presence of increasing amounts of an organic solvent was evaluated by Dynamic Light Scattering (DLS) measurements. The screening was performed considering a set of non-nucleophilic, completely water soluble solvents (dimethylformamide, DMF; dimethylsulphoxyde, DMSO; 2-butanone; acetonitrile). This last characteristic is necessary to form a homogeneous water mixture during the nanoparticle synthesis, while an inert solvent is useful to perform the *in situ* functionalization of the doping agent (dye(s), ligand(s), *etc.*) with trialkoxysilane moieties.

Quite surprisingly, our DLS experiments (Table 2) showed that with the only exception of 2-butanone, Pluronic F127 aggregates maintain characteristics similar to the aggregates formed in pure water up to ~40% V/V concentration of organic solvent. The increase in the organic solvent concentration had only minor effects on the average hydrodynamic diameters of the Pluronic F127 aggregates. In most cases, the derived scattering intensity (DCR) produced by the presence of the surfactant aggregates in solution was comparable to the experimental data measured in 1 M acetic acid. This last evidence is an indication that in the water–organic solvent mixture we tested, the number of Pluronic F127 aggregates formed in the solution and the number of templates available for the nanoparticle formation is rather constant.

### Synthesis of core–shell silica–PEG nanoparticles and core–shell silica–PEG nanoparticles doped with metalloporphyrins

The previous DLS experiments prompted us to verify the formation of core–shell silica–PEG nanoparticles in these new solvent conditions. In the first experiments, we focused on the synthesis of non-doped silica nanoparticles by the addition of tetraethoxysilane (TEOS) as a silica precursor. Table 3 provides an overview of the results that we obtained, and shows that most of the solvent mixtures were suitable to host the formation of silica nanoparticles. The only exception is represented by the more concentrated acetonitrile mixture that did not lead to the formation of a colloidal system due to the formation of a precipitate. A common feature of all the nanoparticle suspensions obtained in these conditions is the relatively good monodispersion (PdI = 0.2) in the entire concentration range we tested for each solvent. In particular, the 2-butanone and acetonitrile systems cause the formation of nanoparticles with average hydrodynamic diameters slightly higher than the ones usually obtained in 1 M acetic acid. Probably because of their much higher polarity, DMSO and DMF cause the formation of nanoparticles with average hydrodynamic diameters that are more similar to the ones obtained in the standard acetic acid conditions.

In the case of luminescent doping agents with poor solubility in the standard 1 M acetic acid aqueous mixture, DMSO and in particular DMF are the more interesting and versatile solvents to use. In particular, DMF is a solvent with very high solubilization capability, and it is also very often the solvent of choice when coupling reactions come into play. In the case of the porphyrin derivatives we tested in this work, DMF represents the best solvent for the solubilization of the porphyrin carboxylic derivatives and for their efficient coupling to 3-aminopropyltriethoxysilane (APTES), using CDMT (2-chloro-4,6-dimethoxy-1,3,5-triazine and NMM (4-methylmorpholine) as coupling reagents. In the preparation of the porphyrin triethoxysilane derivatives, a coupling solvent such as DMF offers the possibility to functionalize the dyes *in situ* and use them in the nanoparticle synthesis without further purification. In the case of porphyrin alkoxysilane derivatives, this feature is extremely valuable since their purification is feasible

**Table 2** DLS data measured for Pluronic F127 micelles ([F127] = 5.1 mM) in different organic solvent–water mixtures

| Solvent | Solvent conc. V/V[a] (%) | $d_H \pm$ SD[b] (nm) | PdI | $d_H$ (volume-based)[c] (nm) | DCR[d] (kcps) |
|---|---|---|---|---|---|
| Acetic acid 1 M | 0 | 18.4 ± 0.4 | 0.63 | 6.4 ± 0.2 | 276 ± 4 |
| 2-Butanone | 1.3 | 37 ± 13 | 0.42 | 6.6 ± 0.2 | 225 ± 6 |
| | 5.2 | 20 ± 2 | 0.64 | 6.6 ± 0.1 | 215 ± 6 |
| | 12.9 | 24 ± 6 | 0.57 | 6.8 ± 0.1 | 228 ± 3 |
| | 38.7 | —[e] | —[e] | —[e] | —[e] |
| Acetonitrile | 1.3 | 23 ± 0.1 | 0.80 | 6.4 ± 0.1 | 318 ± 14 |
| | 5.2 | 21 ± 3 | 0.63 | 6.7 ± 0.1 | 276 ± 25 |
| | 12.9 | 19 ± 4 | 0.43 | 6.5 ± 0.2 | 244 ± 33 |
| | 38.7 | 21.4 ± 0.1 | 0.15 | 17.8 ± 0.2 | 970 ± 14 |
| DMSO | 1.3 | 19 ± 1 | 0.65 | 6.0 ± 0.1 | 280 ± 10 |
| | 3.2 | 22 ± 2 | 0.41 | 9.0 ± 0.3 | 287 ± 10 |
| | 16.1 | 26 ± 3 | 0.56 | 7.1 ± 0.3 | 315 ± 20 |
| | 38.7 | 19 ± 1 | 0.49 | 6.6 ± 0.1 | 310 ± 10 |
| DMF | 1.3 | 19 ± 5 | 0.44 | 6.5 ± 0.2 | 250 ± 30 |
| | 5.2 | 42 ± 17 | 0.42 | 7.0 ± 1 | 370 ± 70 |
| | 12.9 | 24 ± 14 | 0.42 | 7 ± 2 | 230 ± 30 |
| | 38.7 | 16 ± 3 | 0.43 | 7 ± 1 | 240 ± 60 |

[a] V/V% concentration (the total volume for each solution was 1550 μL). [b] Average hydrodynamic diameter distribution by intensity. [c] Average hydrodynamic diameter distribution by volume. [d] Derived scattering intensity measured by the detector. [e] Data not available because of emulsion formation.

Table 3 DLS data measured for Pluronic F127 nanoparticles prepared in different mixtures of organic solvent and 1 M acetic acid mixtures

| Solvent | Solvent conc. V/V[a] (%) | $d_H$ ± SD[b] (nm) | PdI | $d_H$ [c] ((volume-based) ± SD) (nm) |
|---|---|---|---|---|
| Acetic acid 1 M | 0 | 21.2 ± 0.1 | 0.13 | 20.3 ± 0.2 |
| 2-Butanone | 1.3 | 30 ± 1 | 0.13 | 23.2 ± 0.3 |
| | 5.2 | 36.3 ± 0.4 | 0.11 | 30 ± 1 |
| | 12.9 | 26.8 ± 0.4 | 0.15 | 23 ± 2 |
| Acetonitrile | 1.3 | 35.4 ± 0.2 | 0.25 | 34 ± 2 |
| | 5.2 | 31.3 ± 0.1 | 0.22 | 30 ± 1 |
| | 12.9 | 30.6 ± 0.4 | 0.22 | 29 ± 2 |
| | 38.7 | —[d] | —[d] | —[d] |
| DMSO | 1.3 | 36 ± 1 | 0.21 | 20 ± 1 |
| | 3.2 | 17.2 ± 0.3 | 0.21 | 15 ± 1 |
| | 5.2 | 26.6 ± 0.3 | 0.22 | 21.7 ± 0.4 |
| | 12.9 | 21.6 ± 0.2 | 0.22 | 20 ± 2 |
| | 16.1 | 24.0 ± 0.4 | 0.11 | 21.0 ± 0.3 |
| | 38.7 | 24 ± 1 | 0.21 | 22 ± 1 |
| DMF | 1.3 | 20.7 ± 0.3 | 0.18 | 19 ± 1 |
| | 5.2 | 26 ± 1 | 0.36 | 22 ± 1 |
| | 12.9 | 22 ± 2 | 0.22 | 20 ± 2 |
| | 38.7 | 21 ± 1 | 0.18 | 19 ± 2 |

[a] V/V% concentration (the total volume for each solution was 3100 μL). [b] Average hydrodynamic diameter distribution by intensity. [c] Average hydrodynamic diameter distribution by volume. [d] Data not available because of precipitation.

only with tedious size exclusion chromatographic methods. Porphyrins **Pd-1-COOH**, **Pt-2-COOH**, **Pt-3-COOH**, and **Pd-3-COOH** were coupled to APTES and then directly used in the preparation of dye-doped silica nanoparticles in a doping regime of 0.5% (moldye/molTEOS × 100). The morphological characterization performed by DLS analysis (Fig. 2 and Fig. S5–7†) and by TEM microscopy (Fig. 3 and Fig. S8–10†) showed uniform characteristics for all the samples we synthesized in terms of the hydrodynamic diameter and of silica core diameter distributions.

### Photophysical properties of the core–shell silica–PEG nanoparticles doped with metalloporphyrin

In order to evaluate the possible use of silica nanoparticles as oxygen sensors, we first performed their photophysical characterization in aqueous dispersions at room temperature (absorption and emission spectra, luminescence lifetimes) and compared the results with the data obtained for the different free porphyrins in THF because of their insolubility in water.

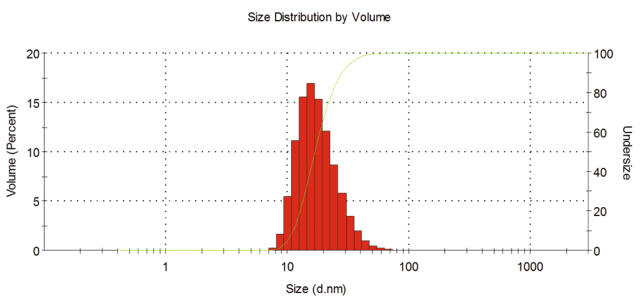


Fig. 2 DLS hydrodynamic distribution by volume of core–shell silica nanoparticles doped with porphyrin **Pd-1-APTES** ($d_H$ = 22 nm, PdI = 0.23, water 25 °C).

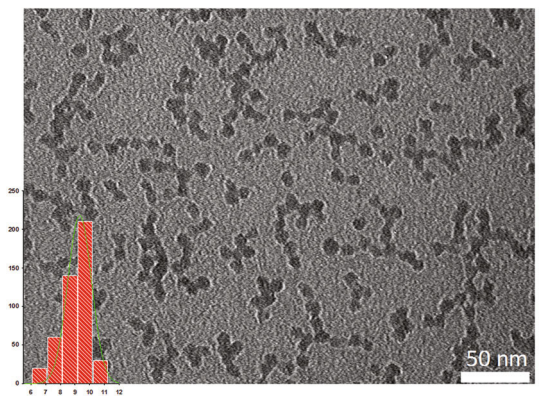


Fig. 3 TEM images and diameter distribution of core–shell silica nanoparticles doped with porphyrin **Pd-1-APTES** ($d_{core}$ = 10 ± 2 nm).

As it can be seen from Fig. 4 (and from Fig. S9–S11†), the shape of the absorption spectrum is often broader than the one of the corresponding free porphyrin for all samples.

We had already observed a similar spectral broadening also when other chromophores (*e.g.* cyanines) were included in the silica core of this kind of NPs. We have explained this effect with their confinement that could cause some degree of aggregation. We were also able to determine the absorption coefficients of the different NPs, measuring their concentration as previously reported[41] and the data are presented in Table 4.

From these values, we have estimated the average number of porphyrins contained in each NP, assuming that the absorption coefficient of each dye remains almost unchanged when inserted in the silica matrix. However, it has to be underlined that this assumption, quite realistic in many cases, is not applicable when aggregation occurs and therefore our results represent only a lower limit, since aggregation typically

 

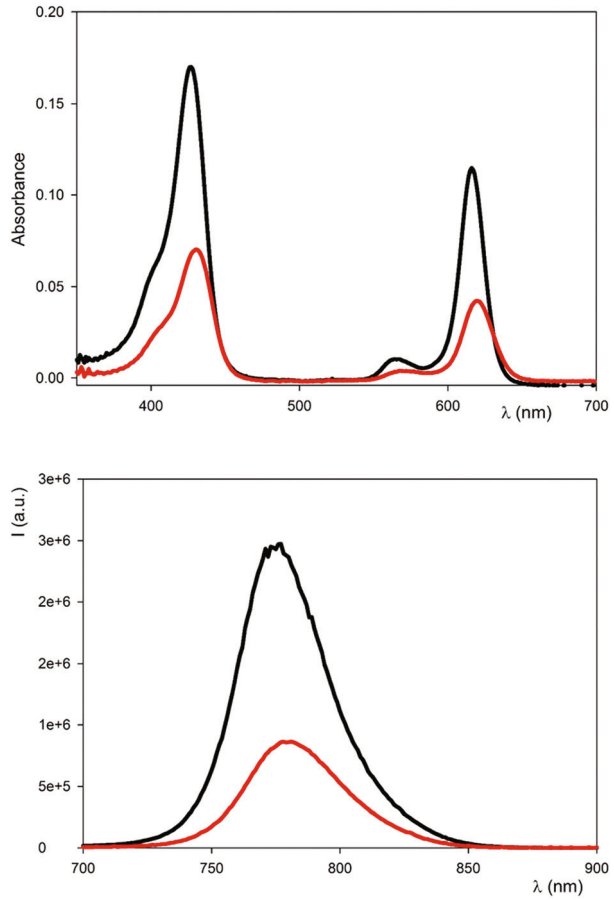


Fig. 4 Absorption (above) and emission (below, $\lambda_{ex}$ = 440 nm) spectra in aerated solutions of **Pt-3-COOH** in THF (black) and nanoparticles doped with **Pt-3-APTES** in water (red). [**Pt-3-COOH**] = 1.46 μM; [**Pt-3-APTES NPS**] = $4 \times 10^{-8}$ M.

reduces the absorption coefficient. In general, however, as it can be observed from the data of Table 4, the molar absorption of the NPs is quite high, exceeding in all cases the value of $1 \times 10^6$ $M^{-1}$ $cm^{-1}$ for their Soret band. Interestingly, also for the weaker Q-bands the observed range is between $4.9 \times 10^5$ and $1.3 \times 10^6$ $M^{-1}$ $cm^{-1}$. The quite high values obtained with this synthetic methodology are an important pre-requisite for many applications related to photochemistry, such as optical and photoacoustic imaging, photothermal and photodynamic therapy, and sensing.

As far as the luminescence spectra are concerned, Pd porphyrins in THF aerated solutions show a fluorescence band with $\lambda_{max}$ = *ca.* 610 nm and *ca.* 640 nm for **Pd-1-COOH** (Fig. S9†) and **Pd-3-COOH** (Fig. S10†), respectively, and a phosphorescence band almost absent for **Pd-1-COOH** and very weak for **Pd-3-COOH**.

In the case of the free Pt porphyrins, the fluorescence is absent while a moderately stronger phosphorescence band can be detected, with $\lambda_{max}$ = 668 and 778 nm for **Pt-2-COOH** (Fig. S11†) and **Pt-3-COOH** (Fig. 4), respectively. The different behaviour observed for the Pd porphyrins with respect to the Pt porphyrins was expected. In fact, there are examples of prompt fluorescence also for other Pd porphyrins, as in the case of PdOEO and PdTPP, while this is typically not true for Pt porphyrins.[42] At the same time, the replacement of Pd by Pt leads to an enhancement of the phosphorescence intensity accompanied by a small blue shift (from 810 to 778 nm for **Pd-3-COOH** and **Pt-3-COOH**). The shift to higher energies can be also typically observed in the absorption spectrum,[42] as again evidenced by the metal-3-COOH compounds (see Fig. 4). As expected, for all four of the porphyrins studied here, the phosphorescence intensities and lifetimes (Table 4) undergo a drastic increase upon de-oxygenation of the solution.

When the metal-porphyrins are conjugated to APTES (chemical structures in Fig. S1–4†) and covalently linked to the silica matrix in the nanoparticles, the phosphorescence bands undergo a small red shift and their measured quantum yields in de-oxygenated solutions are in all cases lower than those of their free counterparts. This behaviour can be very reasonably explained again with the occurrence of self-aggregation inside the silica matrix that usually leads to such an effect. It has to be underlined, however, that despite the decrease observed in these conditions, the NPs – due to their much higher absorption (estimated on a per-particle basis) – are much brighter than free dyes. From the point of view of their potential application as oxygen sensors, air-equilibrated solutions of the NPs

Table 4 Main photophysical data of the metallo-porphyrin and of the luminescent nanoparticles reported in this work. Solvents: metallo-porphyrin, THF; nanoparticles, water

| | Pd-1-COOH | Pd-1-APTES NPs | Pd-3-COOH | Pd-3-APTES NPS | Pt-2-COOH | Pt-2-APTES NPS | Pt-3-COOH | Pt-3-APTES NPS |
|---|---|---|---|---|---|---|---|---|
| $\varepsilon_1$ ($cm^{-1}$ $M^{-1}$) | 415 nm<br>390 000 | 406 nm<br>2 900 000 | 438 nm<br>120 000 | 439 nm<br>1 900 000 | 401 nm<br>240 000 | 401 nm<br>4 700 000 | 429 nm<br>120 000 | 429 nm<br>1 750 000 |
| $\varepsilon_2$ ($cm^{-1}$ $M^{-1}$) | 526 nm<br>35 000 | 526 nm<br>375 000 | 625 nm<br>46 250 | 629 nm<br>750 000 | 511 nm<br>19 500 | 511 nm<br>525 000 | 615 nm<br>78 500 | 619 nm<br>1 050 000 |
| $l_{PHOSP}$ (nm) | 688 | 703 | 805 | 810 | 654 | 664 | 773 | 778 |
| $N°$ dye/NP | — | 11 | — | 17 | — | 27 | — | 14 |
| $d_H$ (nm) | — | 17 | — | 27 | — | 20 | — | 24 |
| $\Phi_{EM}$ deareated (%) | 2.3 | 0.7 | 1.3 | 0.2 | 1.8 | 1 | 2.4 | 1.6 |
| $\Phi_{EM}$ areated (%) | <0.1 | 0.3 | 0.06 | 0.15 | 0.2 | 0.5 | 0.16 | 0.4 |
| $\tau$ deareated (ms) | 0.310 | 0.091 | 0.193 | 0.153 | 0.026 | 0.053 | 0.046 | 0.040 |
| $\tau$ areated (ms) | — | 0.030 | 0.008 | 0.063 | 0.001 | 0.002 | 0.010 | 0.017 |

doped with **Pd-1-APTES**, **Pd-3-APTES** and **Pt-3-APTES** exhibit phosphorescence decay times in the order of 10–-20 microseconds that is similar to those observed for established dendritic oxygen probes.[35,36] Furthermore, as it can be seen in Table 4, the luminescence intensity and lifetime are sensitive to oxygen concentrations, proving that the phosphorescent nanoparticles may exhibit potential for biological oxygen sensing.

## Conclusions

In this work, we have demonstrated the possibility of carrying out synthesis of luminescent silica NPs in organic solvent–water mixtures by using a template-assisted method based on Pluronic F127 micelles. We found that Pluronic F127 aggregates maintain their hydrodynamic properties in water mixtures containing a large amount (up to 40% v/v) of water soluble organic solvents such as DMSO, DMF, acetonitrile or 2-butanone. In these conditions, these aggregates maintain their capability to act as templates for the formation of silica NPs with uniform size, with a hydrodynamic diameter of 25–30 nm. We have demonstrated the feasibility of this approach for the fabrication of silica NPs doped with metallo-porphyrins, with a challenging example of doping NPs with dyes having high hydophobicity and high propensity for aggregation. With our method, it is possible to perform functionalization of the dye with alkoxysilane groups in a strong solubilizing solvent such as DMF, and to directly use this reaction mixture in a one-pot procedure, avoiding the problematic step of purification and isolation of the luminescent metallo-porphyrin dyes. In this way, we were able to obtain NPs presenting properties that are compatible with oxygen sensing in biological environments, *i.e.*, high colloidal stability, appropriate brightness, and efficient shielding from oxygen.

This synthetic strategy should be suitable for the construction of doped nanoparticles for a broad range of applications, such as imaging, sensing, drug delivery, and catalysis, since it reduces the impact of the doping agent solubility on inclusion and silica formation and on the emission properties of the silica nanosystem.

## Conflicts of interest

There are no conflicts to declare.

## Acknowledgements

DG acknowledges Università di Bologna for funding (ALMAIDEA grant). Support of the grants supported by the grants EB018464 and NS092986 (S. A. V.) from the National Institutes of Health, USA is kindly acknowledged. In addition, we kindly acknowledge Nicola Bogo for preliminary experiments.

## Notes and references

1 M. Montalti, L. Prodi, E. Rampazzo and N. Zaccheroni, *Chem. Soc. Rev.*, 2014, **43**, 4243–4268.
2 B. Yang, L. Leclercq, J.-M. Clacens and V. Nardello-Rataj, *Green Chem.*, 2017, **19**, 4552–4562.
3 A. Kausar and T. Iqbal, *Polym.-Plast. Technol. Eng.*, 2016, **55**, 826–861.
4 C. Caltagirone, A. Bettoschi, A. Garau and R. Montis, *Chem. Soc. Rev.*, 2015, **44**, 4645–4671.
5 R. Enrico, G. Damiano, P. Francesco, P. Luca and Z. Nelsi, *Methods Appl. Fluoresc.*, 2018, **6**, 022002.
6 J. Wen, K. Yang, F. Liu, H. Li, Y. Xu and S. Sun, *Chem. Soc. Rev.*, 2017, **46**, 6024–6045.
7 E. Aznar, M. Oroval, L. Pascual, J. R. Murguía, R. Martínez-Máñez and F. Sancenón, *Chem. Rev.*, 2016, **116**, 561–718.
8 S. Bonacchi, D. Genovese, R. Juris, M. Montalti, L. Prodi, E. Rampazzo, M. Sgarzi and N. Zaccheroni, *Top. Curr. Chem.*, 2011, **300**, 93–138.
9 K. Li, J. Wei, H. Yu, P. Xu, J. Wang, H. Yin, M. A. Cohen Stuart and S. Zhou, *Angew. Chem., Int. Ed.*, 2018, **57**, 16458–16463.
10 J. Bourquin, A. Milosevic, D. Hauser, R. Lehner, F. Blank, A. Petri-Fink and B. Rothen-Rutishauser, *Adv. Mater.*, 2018, **30**, e1704307.
11 J. G. Croissant, Y. Fatieiev and N. M. Khashab, *Adv. Mater.*, 2017, **29**, 1604634.
12 J. G. Croissant, Y. Fatieiev, A. Almalik and N. M. Khashab, *Adv. Healthcare Mater.*, 2018, **7**, 1700831.
13 L. Maggini, L. Travaglini, I. Cabrera, P. Castro-Hartmann and L. De Cola, *Chemistry*, 2016, **22**, 3697–3703.
14 L. Maggini, I. Cabrera, A. Ruiz-Carretero, E. A. Prasetyanto, E. Robinet and L. De Cola, *Nanoscale*, 2016, **8**, 7240–7247.
15 W. Stöber, A. Fink and E. Bohn, *J. Colloid Interface Sci.*, 1968, **26**, 62–69.
16 M. Nakamura and K. Ishimura, *Langmuir*, 2008, **24**, 5099–5108.
17 M. S. Bradbury, E. Phillips, P. H. Montero, S. M. Cheal, H. Stambuk, J. C. Durack, C. T. Sofocleous, R. J. C. Meester, U. Wiesner and S. Patel, *Integr. Biol.*, 2013, **5**, 74–86.
18 R. P. Bagwe, L. R. Hilliard and W. Tan, *Langmuir*, 2006, **22**, 4357–4362.
19 R. P. Bagwe, C. Yang, L. R. Hilliard and W. Tan, *Langmuir*, 2004, **20**, 8336–8342.
20 L. Cai, Z.-Z. Chen, M.-Y. Chen, H.-W. Tang and D.-W. Pang, *Biomaterials*, 2013, **34**, 371–381.
21 R. Kumar, I. Roy, T. Y. Ohulchanskky, L. A. Vathy, E. J. Bergey, M. Sajjad and P. N. Prasad, *ACS Nano*, 2010, **4**, 699–708.
22 R. Kumar, I. Roy, T. Y. Ohulchanskyy, L. N. Goswami, A. C. Bonoiu, E. J. Bergey, K. M. Tramposch, A. Maitra and P. N. Prasad, *ACS Nano*, 2008, **2**, 449–456.
23 I. R. Diksha, *Methods Mol. Biol.*, 2012, **906**, 365–379.
24 E. Rampazzo, S. Bonacchi, M. Montalti, L. Prodi and N. Zaccheroni, *J. Am. Chem. Soc.*, 2007, **129**, 14251–14256.

 

25 D. Genovese, S. Bonacchi, R. Juris, M. Montalti, L. Prodi, E. Rampazzo and N. Zaccheroni, *Angew. Chem., Int. Ed.*, 2013, **52**, 5965–5968.
26 E. Rampazzo, S. Bonacchi, D. Genovese, R. Juris, M. Montalti, V. Paterlini, N. Zaccheroni, C. Dumas-Verdes, G. Clavier, R. Méallet-Renault and L. Prodi, *J. Phys. Chem. C*, 2014, **118**, 9261–9267.
27 E. Rampazzo, R. Voltan, L. Petrizza, N. Zaccheroni, L. Prodi, F. Casciano, G. Zauli and P. Secchiero, *Nanoscale*, 2013, **5**, 7897–7905.
28 E. Rampazzo, F. Boschi, S. Bonacchi, R. Juris, M. Montalti, N. Zaccheroni, L. Prodi, L. Calderan, B. Rossi, S. Becchi and A. Sbarbati, *Nanoscale*, 2012, **4**, 824–830.
29 M. Helle, E. Rampazzo, M. Monchanin, F. Marchal, F. Guillemin, S. Bonacchi, F. Salis, L. Prodi and L. Bezdetnaya, *ACS Nano*, 2013, **7**, 8645–8657.
30 S. Biffi, L. Petrizza, C. Garrovo, E. Rampazzo, L. Andolfi, P. Giustetto, I. Nikolov, G. Kurdi, M. B. Danailov, G. Zauli, P. Secchiero and L. Prodi, *Int. J. Nanomed.*, 2016, **11**, 4865–4874.
31 E. Rampazzo, S. Bonacchi, R. Juris, D. Genovese, L. Prodi, N. Zaccheroni and M. Montalti, *Chem. – Eur. J.*, 2018, **24**, 16743–16746.
32 G. Valenti, E. Rampazzo, S. Bonacchi, L. Petrizza, M. Marcaccio, M. Montalti, L. Prodi and F. Paolucci, *J. Am. Chem. Soc.*, 2016, **138**, 15935–15942.
33 J. M. Vanderkooi, G. Maniara, T. J. Green and D. F. Wilson, *J. Biol. Chem.*, 1987, **262**, 5476–5482.
34 W. L. Rumsey, J. M. Vanderkooi and D. F. Wilson, *Science*, 1988, **241**, 1649–1651.
35 A. Y. Lebedev, A. V. Cheprakov, S. Sakadžić, D. A. Boas, D. F. Wilson and S. A. Vinogradov, *ACS Appl. Mater. Interfaces*, 2009, **1**, 1292–1304.
36 T. V. Esipova, A. Karagodov, J. Miller, D. F. Wilson, T. M. Busch and S. A. Vinogradov, *Anal. Chem.*, 2011, **83**, 8756–8765.
37 S. A. Vinogradov and D. F. Wilson, in *Designing Dendrimers*, ed. S. Campagna and P. Ceroni, Wiley, New York, 2012.
38 T. V. Esipova, M. J. P. Barrett, E. Erlebach, A. E. Masunov, B. Weber and S. A. Vinogradov, *Cell Metab.*, 2019, **29**, 736–744.
39 M. Quaranta, S. M. Borisov and I. Klimant, *Bioanal. Rev.*, 2012, **4**, 115–157.
40 D. B. Papkovsky and A. V. Zhdanov, *Free Radicals Biol. Med.*, 2016, **101**, 202–210.
41 E. Rampazzo, S. Bonacchi, R. Juris, M. Montalti, D. Genovese, N. Zaccheroni, L. Prodi, D. C. Rambaldi, A. Zattoni and P. Reschiglian, *J. Phys. Chem. B*, 2010, **114**, 14605–14613.
42 *Photochemistry of polypyridine and porphyrin complexes*, ed. K. Kalyanasundaram, Academic Press, London, 1992.